Modeling and Design of Exhaust Manifold Under Thermomechanical Loading

K.H. Park[1], B.L. Choi[1], K.W. Lee[1], K.-S. Kim[2] and Y.Y. Earmme[3]*

[1]Vehicle Development & Analysis Team, Research & Development Division, Hyundai-Motor

Company, Korea

[2]Division of Engineering, Brown University, U.S.A.

[3]Department of Mechanical Engineering, Korea Advanced Institute of Science and Technology,

Daejeon, Korea

_____

*Corresponding author:

Address : Y.Y. Earmme, Department of Mechanical Engineering, KAIST, 373-1, Guseong-dong,

Yuseong-gu, Daejeon, 305-701, Korea

Tel   : +82-42-869-3013

Fax   : +82-42-869-3210

e-mail   : y.y.earmme@kaist.ac.kr

Abstract: In the early stage of designing the exhaust manifold, a designer usually has to perform the fatigue analysis of each candidate of the exhaust manifold, and to decide whether or not it is satisfactory. In each case, the elasto-plastic stress analysis by F.E.M. is required, which is very time-consuming considering the pre-processing and post-processing of the F.E.M data. In this study, a thermal stress index (TSI) is proposed for a practical application to the early stage of designing the exhaust manifold. Although this index, a ratio of the elastic effective stress to yield stress, does not predict quantitatively the expected fatigue life, it is believed that this index can be relatively easily evaluated, and its merit lies in the quick estimation of the effect of the design parameters at the development stage with comparing the nonlinear fatigue analysis.

NOTATION

A	junction point of cylinder head and end point of exhaust pipe
A_o	area of cross section
$\hat{A}$	effective area of cylinder head
a_i	direction cosine to the coordinate $(i = 1,2,3)$
B	arbitrary point B in a curved member
$\mathbf{C}$	compliance matrix for exhaust pipe
$\hat{\mathbf{C}}$	compliance matrix for cylinder head
D_o	diameter of exhaust pipe

D	generalized displacement matrix for exhaust pipe
D̂	generalized displacement matrix for cylinder head
E	Young's modulus of exhaust pipe
$\hat{E}$	longitudinal modulus of cylinder head
$\boldsymbol{e}_u$	unit vector in the direction of the line made by junction points of exhaust pipe
$\boldsymbol{e}_i$	unit vector of the coordinate
F	generalized force matrix
$\boldsymbol{f}$	force vector
G	shear modulus
$\boldsymbol{g}_A$	geometry function
I_o	2nd moment of inertia
I	unit matrix
J	polar moment of inertia
K̂	stiffness matrix for cylinder head
K̂$^{-1}$	inverse of stiffness matrix for cylinder head
k	spring constant of cylinder head between p^{th} and $(\text{p}+1)^{\text{th}}$ junction points
L	normal length from cylinder head to point O
l	length between p^{th} and $(\text{p}+1)^{\text{th}}$ junction points
ℓ	total length of exhaust pipe
M	bending moment
$\boldsymbol{m}$	moment vector
N	axial force
O	point collecting exhaust pipes (origin of the coordinate system)
R	half length of cylinder head used in verification program

$\boldsymbol{r}_A$	position vector of the point A.
$\boldsymbol{r}(s)$	position vector of B
s	The length from point O to point B
$\boldsymbol{T}$	twisting moment
T	temperature
$T(s)$	temperature at point B,
T_R	ambient temperature
TSI	thermal stress index
t	thickness of exhaust pipe
$\boldsymbol{U}_A$	displacement vector at point A (junction point)
$\boldsymbol{U}_R$	displacement vector at reference point in cylinder head
$\hat{\boldsymbol{U}}_T$	displacement vector by thermal expansion of the cylinder head
$\boldsymbol{u}$	displacement vector of exhaust pipe
$\hat{\boldsymbol{u}}$	displacement vector of cylinder head
$\boldsymbol{X}_R$	displacement vector of the reference point in cylinder head
V	lateral force
ρ	twisting angle
χ	shear coefficient
$\tilde{\boldsymbol{K}}$	principal normal vector (or curvature vector)
α	thermal expansion coefficient of exhaust pipe
$\hat{\alpha}$	thermal expansion coefficient of cylinder head
ε_T	axial strain
ε_N	lateral strain
$\boldsymbol{\xi}(s)$	unit tangent vector at point B

Φ strain energy stored in the exhaust pipe

σ normal stresses at the outer point of cross section of exhaust pipe

σ_y yield strength in simple tension

τ shear stresses at the outer point of cross section of exhaust pipe

τ_{eq} equivalent stress

τ_y yield strength in simple shear

$\boldsymbol{\omega}$ rotation angle vector of exhaust pipe

$\hat{\boldsymbol{\omega}}$ rotation angle vector for cylinder head

Superscript

p, q p^{th}, q^{th} exhaust pipe

$\wedge$ values at cylinder head

Subscript

i, j, k i^{th}, j^{th} and k^{th} component

A point A

O point O

1 INTRODUCTION

The exhaust manifold mounted on the cylinder head of an engine collects a gas exhausted from an engine, and sends it to a catalyst converter. The exhaust manifold plays an important role in the performance of an engine system. Particularly, the efficiencies of emission and fuel consumption are closely related to the exhaust manifold. The exhaust manifold is under a thermal fatigue produced by increasing and decreasing temperature, which leads to a crack of the exhaust manifold.

Thermal and mechanical loadings are generally known as major factors in the failure of the exhaust manifold. A special attention has been focused on the low cycle thermal fatigue by accelerated laboratory tests[1] and by FEM or analytical methods[2-5] for evaluating life performance of the exhaust manifold under a cyclic thermal loading. Through a great deal of efforts to increase the performance and to reduce the weight, automotive companies have tried to achieve a goal in optimal engine design.

Shimizu[6] obtained a distributed thermal loading by using a three-dimensional engine cycle and thermal flow simulations to analyze the deformation behaviors under a thermal shock, considering thermo-elastoplasticity. Kazuo et al.[7] used the simple restraint ratio in order to evaluate some parameters for the thermal fatigue durability of the exhaust manifold. (restraint ratio was defined to be that of the difference between the exhaust pipes' thermal expansion with and without restraint by the exhaust manifold to the free expansion under a given temperature difference.) Wolff[8] concluded that the mechanical stresses induced by the vibration of the exhaust system do not yield a major effect on the fatigue life of the exhaust manifold.

A number of engineers have tried to determine the fatigue life of a structure in engineering use. An advanced technique to estimate the fatigue life is the elastic-plastic finite element

analysis which requires at least several days of computing time (including pre and post-processing time) with a modern computer to simulate the exhaust manifold. Moreover material properties, loading conditions, manufacturing processes, surface roughness and welding conditions lead to a significant difference in the evaluation of the fatigue life. In addition the change of the shape of the exhaust manifold is tried at least 10 times in design process. Consequently the elastic-plastic analysis is impractical in design process, and the linear elastic analysis for several candidates has been carried out to select one with a relatively low stress. In particular the optimization for the shape of a complex exhaust manifold with several hundred thousands of finite elements is very difficult to perform in order to meet a tight design schedule.

In this paper, thermal stress index (TSI) is developed for practical purpose. Particularly the TSI is shown to be very effective in finding an optimal shape with constraints in design of the exhaust manifold. As a result, the final goal for finding an optimal shape of the exhaust manifold is to minimize the TSI.

2 FORMULATION OF THE THERMAL STRESS (TSI)

2.1 SIMPLIFIED MODEL OF EXHAUST MANIFOLD

The exhaust manifold consists of inlet flange, exhaust pipes (or sometimes called runners) and outlet flange. To simplify the exhaust manifold model, the exhaust pipe is assumed to be a curved beam member as shown in Fig. 1. The path of the beam follows the center line of the pipe. The point O collecting the exhaust pipes is at the origin of the coordinate system. The sequence of the pipe number starts from the left, and the junction points ①~④ of the exhaust pipes are located on the same line whose unit vector is $e_u = a_i e_i$, where a_i $(i = 1,2,3)$ is a direction cosine to the coordinate. X_R on the cylinder head is the reference point for the displacements. The position of the junction of the cylinder and the pth pipe end is r_A^p.
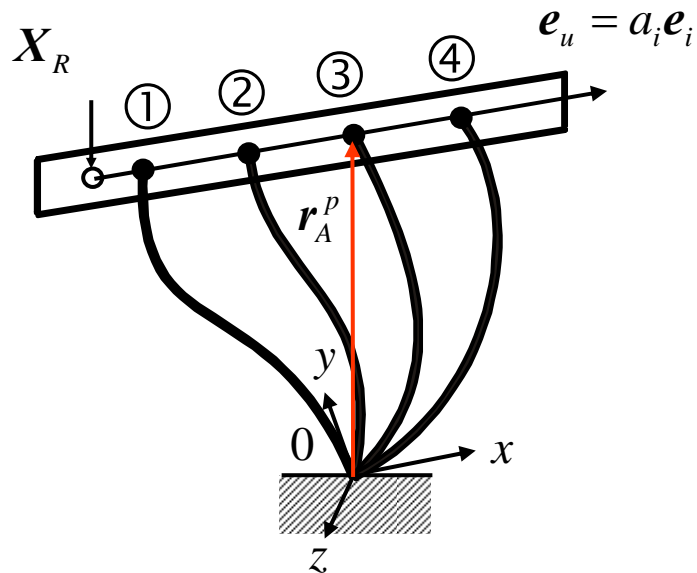
Fig. 1 Schematic configuration of the simplified exhaust manifold

2.2 THERMAL DEFORMATIONS OF EXHAUST PIPE

2.2.1 THERMAL DEFORMATIONS OF A CURVED BEAM

In order to know the behavior of the exhaust manifold system, we first consider an exhaust pipe treated as a curved member having a total length of ℓ (from O to A) with the end free at A and fixed at O as shown in Fig. 2.
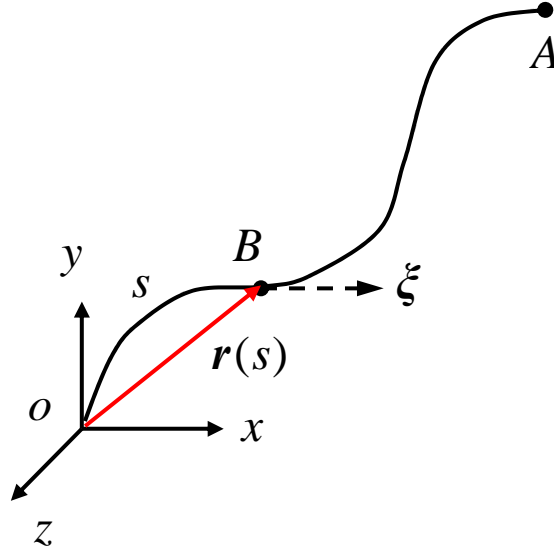
Fig. 2 A curved member in a space

The length from point O to an arbitrary point B in the curved member is denoted by s, and the position vector of B, by $r(s)$. Thermal expansion of the member OB causes an infinitesimal movement of the free end point A as well as point B, and the infinitesimal displacement at A is written as

$$d\boldsymbol{u} = \alpha\big[T(s) - T_R\big]ds\,\frac{d\boldsymbol{r}(s)}{ds}$$

$$= \alpha T(s)\boldsymbol{\xi}(s)ds - \alpha T_R\boldsymbol{\xi}(s)ds \tag{1}$$

where, α, $\boldsymbol{\xi}(s) = d\boldsymbol{r}(s)/ds$, $T(s)$ and T_R are the thermal expansion coefficient, unit

tangent vector at point B and temperature at point B, and ambient temperature, respectively.

The displacement at point A can be obtained by integrating equation (1) for the total length of a curved member as follows:

$$U_A = \int_O^A du = \alpha \int_O^A T(s)\xi(s)ds - \alpha T_R \int_O^A \xi(s)ds \tag{2}$$

Suppose the linear temperature distribution is given along a curved member as

$$T(s) = T_O + (T_A - T_O)\frac{s}{\ell} \tag{3}$$

where T_O is the temperature at the starting point O, T_A is the temperature at the end point A. Substituting equation (3) into equation (2), one obtains

$$U_A = \alpha(T_A - T_R)r_A - \alpha(T_A - T_O)g_A \tag{4}$$

where, r_A is the position vector of the point A. g_A is a geometry function defined as

$$g_A = \frac{1}{\ell}\int_0^A r(s)ds . \tag{5}$$

Later in this study, we will express $r(s)$ in terms of a polynomial function of s.

2.2.2 COMPLIANCE OF A CURVED MEMBER

The relation between generalized forces ($\mathbf{F}$) and generalized displacements ($\mathbf{D}$) in an elastic system is expressed as

$$\mathbf{D} = \mathbf{C} \cdot \mathbf{F} \tag{6}$$

with 6×6 compliance matrix $\mathbf{C}$, where F_i ($i = 1,2,3$) is a force component f_i ($i = 1,2,3$), while F_i ($i = 4,5,6$) is a moment component m_i ($i = 1,2,3$) and D_i ($i = 1,2,\cdots,6$) is the corresponding generalized displacement (i.e. $u_i = D_i$ ($i = 1,2,3$), $\omega_i = D_{i+3}$ ($i = 1,2,3$)). The components of the compliance matrix can be obtained by taking derivatives of the strain energy with respect to the forces and moments

$$C_{ij} = \frac{\partial^2 \Phi}{\partial F_i \partial F_j} \quad (i, j = 1,2,\cdots,6), \tag{7}$$

where,

$$\Phi = \frac{1}{2}\int_O^A \frac{N^2}{EA_o}ds + \frac{1}{2}\int_O^A \frac{V^2}{\chi GA_o}ds + \frac{1}{2}\int_O^A \frac{M^2}{EI_o}ds + \frac{1}{2}\int_O^A \frac{T^2}{GJ}ds . \tag{8}$$

Hence it is found (the details are in Appendix) that

$$
C_{ij}\big|_{i,j=1,2,3} = \int_O^A \frac{\xi_i \xi_j}{EA_o} ds + \int_O^A \frac{(\delta_{ij} - \xi_i \xi_j)}{\chi GA_o} ds
$$

$$
+ \int_O^A \frac{(\boldsymbol{R}_A)_l (\boldsymbol{R}_A)_l \delta_{ij} - (\boldsymbol{R}_A)_i (\boldsymbol{R}_A)_j}{EI} ds \tag{9a}
$$

$$
+ \int_0^A (\frac{1}{GJ} - \frac{1}{EI}) \varepsilon_{imn} \varepsilon_{jkl} \xi_m \xi_k (\boldsymbol{R}_A)_l (\boldsymbol{R}_A)_n ds,
$$

$$
C_{ij}\big|_{\substack{i=1,2,3 \\ j=4,5,6}} = \int_O^A \frac{\varepsilon_{i(j-3)k}(\boldsymbol{R}_A)_k}{EI} ds
$$

$$
+ \int_O^A (\frac{1}{GJ} - \frac{1}{EI}) \varepsilon_{ikl} \xi_{(j-3)} \xi_k (\boldsymbol{R}_A)_l ds, \tag{9b}
$$

$$
C_{ij}\big|_{i,j=4,5,6} = \int_O^A \frac{\delta_{(i-3)(j-3)}}{EI} ds + \int_O^A (\frac{1}{GJ} - \frac{1}{EI}) \xi_{(i-3)} \xi_{(j-3)} ds \tag{9c}
$$

where, $(\boldsymbol{R}_A)_i$ $(i=1,2,3)$ is the ith component of $\boldsymbol{R}_A = \boldsymbol{r}_A - \boldsymbol{r}(s)$, and E, G, A_o and χ

respectively are the Young's modulus, shear modulus, area of cross section, and shear

coefficient.

2.3 STIFFNESS OF THE CYLINDER HEAD

We now consider the stiffness of the cylinder head. To derive the compliance matirx of the

cylinder head, the followings are assumed in the present study:

(1) Deformations of the cylinder head due to bending moments are negligible because a flexural

modulus of the cylinder head is much larger than those of the exhaust pipes.

(2) The cylinder head only deforms along the direction $\boldsymbol{e}_u$ as in Fig. 1.

As a result, the cylinder head can be simplified by a series of springs as shown in Fig. 3

whose spring constant and length are k^p and l^p, respectively. The forces and displacements

at the junction points of the cylinder head and the exhaust pipes are denoted by $\boldsymbol{F}^p$ and $\hat{\boldsymbol{u}}^p$,

respectively. Denoting by $\hat{E}$ the longitudinal modulus, and by $\hat{A}$ effective area,

$$F^1,\hat{u}^1 \qquad F^2,\hat{u}^2 \qquad F^3,\hat{u}^3 \qquad F^4,\hat{u}^4$$

$$k^1 \qquad k^2 \qquad k^3 \qquad k^4$$
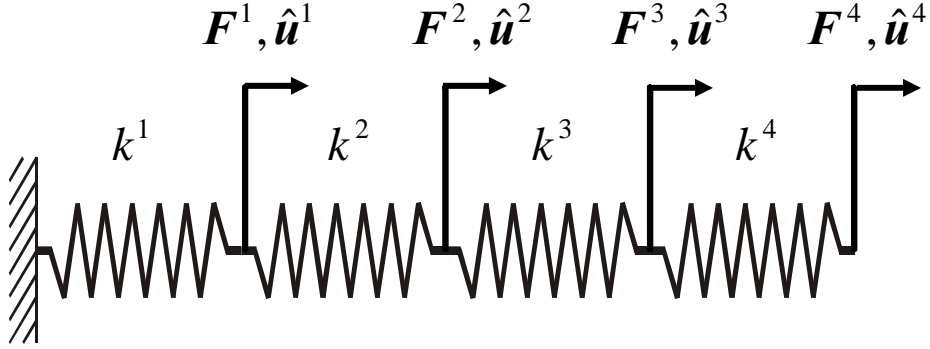
Fig. 3 Schematic diagram of the cylinder head

the forces F_u^p and the displacement $\hat{u}_u^p$, in the direction of $\boldsymbol{e}_u$ (Fig. 1) for the system can be

written by

$$\hat{u}_u^p = \hat{K}_{pq}^{-1} F_u^q. \tag{10}$$

where $p, q = 1, 2, \cdots, N$ is the designation number of the exhaust pipe. The stiffness matrix of

the cylinder head having 4 exhaust pipes by using the spring system shown in Fig. 3 is obtained

as

$$\hat{\mathbf{K}} = \begin{bmatrix} k^1 + k^2 & -k^2 & & \\ -k^2 & k^2 + k^3 & -k^3 & \\ & -k^3 & k^3 + k^4 & -k^4 \\ & & -k^4 & k^4 \end{bmatrix}. \tag{11}$$

The inverse matrix is given by

$$
\hat{\mathbf{K}}^{-1} = \frac{1}{\hat{E}\hat{A}}
\begin{bmatrix}
l^1 & l^1 & l^1 & l^1 \\
l^1 & l^1+l^2 & l^1+l^2 & l^1+l^2 \\
l^1 & l^1+l^2 & l^1+l^2+l^3 & l^1+l^2+l^3 \\
l^1 & l^1+l^2 & l^1+l^2+l^3 & l^1+l^2+l^3+l^4
\end{bmatrix} .
\tag{12}
$$

Since, $\hat{u}_u^p = \hat{\boldsymbol{u}}^p \cdot \boldsymbol{e}_u = (\hat{u}_i^p \boldsymbol{e}_i) \cdot (a_j \boldsymbol{e}_j) = a_i \hat{u}_i^p$ and $F_u^q = \boldsymbol{F}^q \cdot \boldsymbol{e}_u = (F_i^q \boldsymbol{e}_i) \cdot (a_j \boldsymbol{e}_j) = a_j F_j^q$,

the displacements $\hat{u}_i^p$ and forces F_i^p at the junction points of the cylinder head and the

exhaust pipes is rewritten as

$$
\hat{u}_i^p = \hat{K}_{pq}^{-1} a_i a_j F_j^q = \hat{C}_{ij}^{pq} F_j^q \quad (i, j = 1,2,3) .
\tag{13}
$$

And the compliance matrix of the cylinder head is given as $\hat{C}_{ij}^{pq} = \hat{K}_{pq}^{-1} a_i a_j$.

2.4 CONSTITUTIVE EQUATION OF THE EXHAUST MANIFOLD

The forces and moments acting at the joints of the exhaust pipe and the cylinder head, which

are the ends of the exhaust pipes, are related to the combined behavior of exhaust pipes and the

cylinder head. It is therefore required to consider their constitutive and force equilibrium

equations for the evaluation of the stresses in the exhaust pipes.

1) Constitutive equations of the exhaust pipes and the cylinder head:

$$D_i^{\ p} = C_{ij}^{\ \ p} F_j^{\ p}, \qquad (i, j = 1,2,\cdots,6) \quad \text{from equation (6) at the junction}$$

$$\text{of the } p^{th} \text{ pipe (no sum on } p). \tag{14a}$$

$$\hat{D}_i^{\ p} = \hat{C}_{ij}^{\ pq} F_j^{\ q}, \qquad (i, j = 1,2,3) \quad \text{for cylinder head at the } p^{th} \text{ junction} \tag{14b}$$

2) Compatibility condition:

$$D_i^p = \hat{U}_i^{\ p} + (\hat{U}_T^{\ p})_i, \qquad (i = 1,2,3) \tag{15a}$$

$$D_{i+3}^p = \hat{\omega}_i, \qquad (i = 1,2,3) \tag{15b}$$

3) Equilibrium equation:

$$\sum_{p=1}^{N} F_i^{\ p} = 0, \qquad (i = 1,2,3) \tag{16a}$$

$$\sum_{p=1}^{N} \left[F_{i+3}^p + \varepsilon_{ijk} (r_A)_j^p F_k^{\ p} \right] = 0, \quad (i, j, k = 1,2,3) \quad \text{(no sum on } p). \tag{16b}$$

Here $\hat{\omega}$ in equation (15b) represents the rigid body rotation of cylinder head, $D_i^p (i = 1,2,\cdots,6) = \left[u_j^p, \omega_j^p \right]^T (j = 1,2,3)$, $\hat{D}_i^p = \hat{u}_i^p (i = 1,2,3)$ in equations (14a), (14b), and (15a), where the superscript $\hat{}$ represents the value at the cylinder head. Since in formulating $\hat{D}_i^p$, the thermal expansion is not taken into acccount, the thermal displacement $(\hat{U}_T^{\ p})_i$, of the cylinder head is added on the right hand side of equation (15a). The displacements at the junction points of exhaust pipe and the cylinder head are expressed by

$$\hat{U}_i^{\ p} = (U_R)_i + \varepsilon_{ijk} \hat{\omega}_j (r_A^{\ p} - X_R)_k$$

$$+\hat{\alpha}(T_A - T_R) \cdot (\mathbf{r}_A^p - \mathbf{X}_R)_i + \hat{C}_{ij}^{pq} F_j^p \quad (i, j, k = 1,2,3) \tag{17}$$

where $\mathbf{U}_R$ represents the rigid body translation. Substituting equations (14a), (14b) and (17) into equation (15a), one obtains the following expression:

$$C_{im}^p F_m^p - \hat{C}_{ij}^{pq} F_j^q - (\mathbf{U}_R)_i - \varepsilon_{ijk} \hat{\omega}_j (\mathbf{r}_A^p - \mathbf{X}_R)_k$$

$$= \hat{\alpha}(T_A - T_R)(\mathbf{r}_A^p - \mathbf{X}_R)_i + (\hat{\mathbf{U}}_T^p)_i. \tag{18}$$

where the subscript $i, j, k = 1,2,3$ and $m = 1,2,\cdots,6$ and no sum on p in $C_{im}^p F_m^p$ is implied while sum on q is implied. Consequently, The 12 unknowns, which are the forces $f_i = F_i (i = 1,2,3)$, moments $m_i = F_{i+3}(i = 1,2,3)$, displacements $(\mathbf{U}_R)_i (i = 1,2,3)$ and rotation angle $\hat{\omega}_i (i = 1,2,3)$ at each pth junction, can be obtained by simultaneously solving equations (15b), (16a), (16b) and (18).

2.5 MAXIMUM STRESS AND THERMAL STRESS INDEX (TSI)

The stresses at an arbitrary cross section of the exhaust pipes can be calculated by using the forces and moments presented in the previous section. The exhaust manifold system has the highest temperature and the maximum stresses at point O in Fig. 1, which has been confirmed by the results not shown here. We will therefore confine our discussion of the stresses to those at the cross section containing O.

Fig. 4 shows the coordinate system and unit vectors on the cross section of an exhaust pipe at the collecting area. The unit vector $\mathbf{e}_l$ is perpendicular to the tangent vector at O, $\boldsymbol{\xi}_0$, (i.e.

$e_l \perp \boldsymbol{\xi}_0$) and is uniquely determined such that $\boldsymbol{m}_0$ is decomposed into $\boldsymbol{m}_n$ $(// \boldsymbol{\xi}_o)$ and $\boldsymbol{m}_l$. The unit vector $\boldsymbol{e}_m$ is then defined by the vector perpendicular to both $\boldsymbol{\xi}_0$ and $\boldsymbol{e}_l$. (i.e. $\boldsymbol{e}_m \perp \boldsymbol{\xi}_0$ and $\boldsymbol{e}_m \perp \boldsymbol{e}_l$).
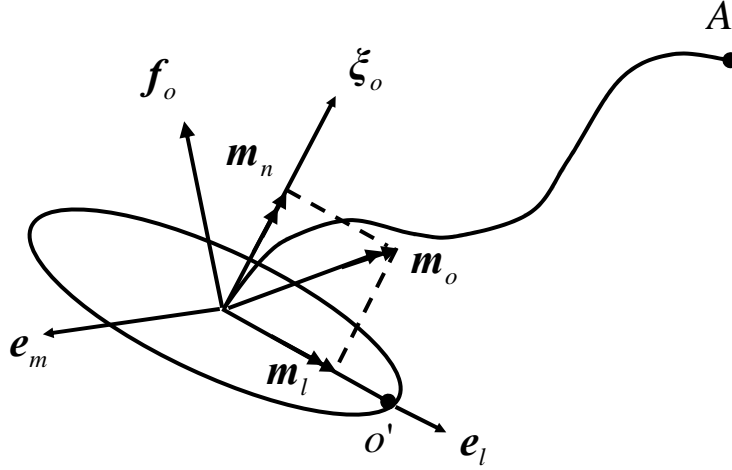
Fig. 4 Definition of the coordinate axis

Force $\boldsymbol{f}_O$ and moment $\boldsymbol{m}_O$ acting on the cross section including the point O can be easily expressed in terms of the force $\boldsymbol{f}_A^p$ and moment $\boldsymbol{m}_A^p$ at point A for each pipe which were already obtained in section 2.4. (the subscript A was omitted there)

$$\boldsymbol{f}_O = \boldsymbol{f}_A^p, \qquad \boldsymbol{m}_O = \boldsymbol{m}_A^p + \boldsymbol{r}_A^p \times \boldsymbol{f}_A^p, \qquad \text{(no sum on } p) \tag{19}$$

Therefore we can write

$$\boldsymbol{m}_l = \boldsymbol{m}_o \cdot \{\mathbf{I} - (\boldsymbol{\xi}_o \otimes \boldsymbol{\xi}_o)\} \tag{20}$$

$$\boldsymbol{m}_n = \boldsymbol{m}_o \cdot (\boldsymbol{\xi}_o \otimes \boldsymbol{\xi}_o) \tag{21}$$

$$e_l = \frac{m_l}{|m_l|} = \frac{m_o}{|m_l|} \cdot \{\mathbf{I} - (\xi_o \otimes \xi_o)\} \tag{22}$$

and $\mathbf{I}$ is the unit matrix. The shear and normal stresses at the outermost point of cross section can be expressed by

$$
\begin{aligned}
\tau^p &= -\frac{m_n \cdot D_o}{2J} + \frac{1}{A_o}(f_o \cdot e_l)\sin(\theta) + (f_o \cdot e_m)\sin(\theta + \frac{\pi}{2}) \\
&= -\frac{m_n \cdot D_o}{2J} + \frac{m_o \cdot \{\mathbf{I} - (\xi_o \otimes \xi_o)\} \cdot f_o}{A_o |m_o \cdot \{\mathbf{I} - (\xi_o \otimes \xi_o)\}|}\sin(\theta) \\
&\quad + \frac{f_o \cdot [m_o \cdot \{\mathbf{I} - (\xi_o \otimes \xi_o)\}] \times \xi_o}{A_o |m_o \cdot \{\mathbf{I} - (\xi_o \otimes \xi_o)\}|}\sin(\theta + \frac{\pi}{2})
\end{aligned}
\tag{23}
$$

$$\sigma^p = \frac{f_o \cdot \xi_o}{A_o} + \frac{D_o |m_o \cdot \{\mathbf{I} - (\xi_o \otimes \xi_o)\}|}{2I_o} \cdot \sin(\theta) \tag{24}$$

where θ is measured from point o' in Fig. 4.

The equivalent stress τ_{eq} is defined by

$$\tau_{eq} = \sqrt{\left(\frac{\sigma^p}{2}\right)^2 + \left(\tau^p\right)^2} \; . \tag{25}$$

The choice of the equivalent stress as in equation (25) or the alternative equivalent stress, τ_{eq} (von Mises), is immaterial as can be seen in the subsequent part of this study. In this study, the thermal stress index (TSI) is now defined as

$$TSI = \frac{\tau_{eq}}{\tau_y} = \frac{2\tau_{eq}}{\sigma_y} = \frac{2}{\sigma_y}\sqrt{\left(\frac{\sigma^p}{2}\right)^2 + \left(\tau^p\right)^2} \qquad (26)$$

where, σ_y is the yield strength of the material used for the pipes at the temperature T_O.

The value TSI as defined by equation (26) is a function of each point at the pipe. As stated earlier, the maximum TSI occurs at the section containing point O. Therefore we compute TSI at the outermost points of the section as a function of θ, and look for a point at which TSI is maximum.

3 APPLICATIONS OF TSI IN THE EXHAUST MANIFOLD

3.1 ANALYSIS MODEL FOR VERIFICATION OF TSI

An arbitrary-shaped exhaust manifold system in a three-dimensional space is examined to show the validity of TSI by comparing the FEM and analytical results. The system shown in Fig. 5 is chosen for this purpose. It is symmetric with repect to yz-plane. An exhaust manifold usually has 3 or 4 exhaust pipes, and we formulated TSI and computed the result with 4 pipes (with the shapes normally used in industry), and it is found that the maximum TSI occurs at the outermost pipe. Therefore, from now on we present the result with 2 pipes as shown in Fig. 5. The temperature of the pipes at the cylinder head T_A linearly increases along the pipe up to the maximum value T_O at point O. The geometrical values, temperatures, and material properties (SUS429[9]) used in the model are listed in Table. 1. The values T_A and T_O are the typical temperatures in industry use.
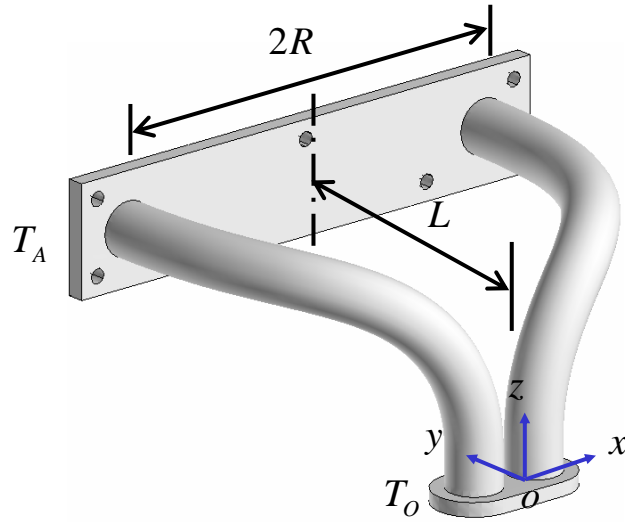
Fig. 5 Geometry of exhaust manifold for analysis

Table 1. Data of the exhaust manifold used in verification program

Geometry		Temperature		Material Property (SUS429 [9])	
R	144mm	T_A	200℃	E	193 (GPa)
L	200mm	T_O	800℃	σ_y (800℃)	23 (MPa)
t	2.0mm	T_R	20℃	σ_y (20℃)	336 (MPa)
D_o	36.5mm			$\hat{\alpha} = \alpha$	10.4×10^{-6} (1/K)

3.2 CALCULATION OF TSI

3.2.1 PRESENT FORMULATION

The schematic positions of the path data for the exhaust pipe are shown in Fig. 6. The total length of ℓ is 354mm and the coefficients of 4th-order-polynomial representing the shape of

the exhaust pipes to be used in equations (5), (9a), (9b) and (9c) are calculated as

$$r_x(s) = 149.3s - 1191.6s^2 + 1448.5s^3 - 531.2s^4,$$ (27a)

$$r_y(s) = 25.2s - 259.3s^2 + 956.8s^3 - 522.7s^4,$$ (27b)

$$r_z(s) = 345.9s + 166.8s^2 - 842.7s^3 + 480.0s^4.$$ (27c)

The displacement at point O is fixed as explained in the section 2.2.1. and the temperature varies linearly along the pipe from T_A (200℃) to T_O (800℃) using equation (3). The compliance matrix $\mathbf{C}$ is calculated by substituting equations (27a), (27b) and (27c) into equations (9a), (9b) and (9c) and the forces and moments at the junction points are obtained by solving equations (15b), (16a), (16b) and (18) with $\mathbf{C}$ and $\hat{\mathbf{C}}$. Then, one finds the stresses at a cross section at O to evaluate TSI from equations (23) and (24). The shear stress along the circumferential direction shows the maximum value at 90° and 270°, and the normal stress has the maximum tension and compression at 90° and 270°, repectively. (not shown here)

The TSI at the outermost points of the cross section at O as a function of θ is shown in Fig. 7. The maximum TSI occurs at $\theta = 270^o$, and it is about 7.014.
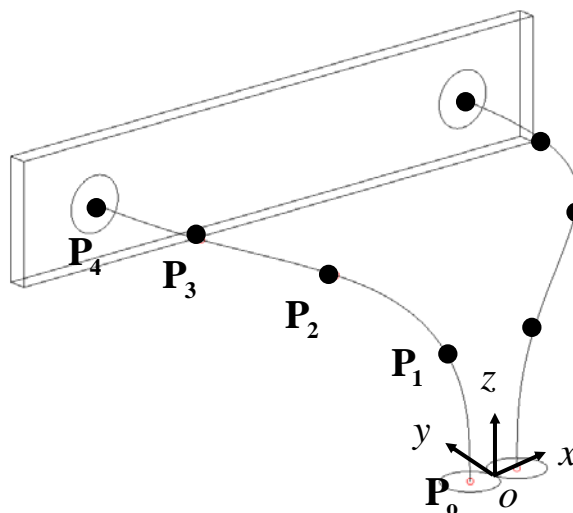
Fig. 6 The geometry of the exhaust pipe for the calculation of TSI
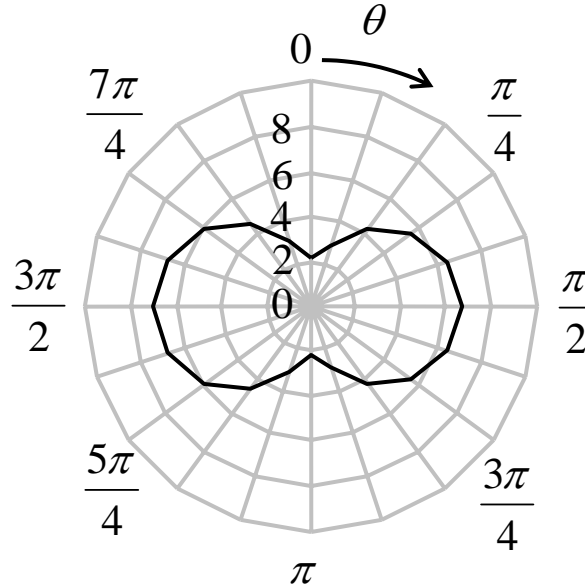
Fig. 7 Thermal fatigue damage index number

3.2.2 FEM ANALYSIS

A linear-elastic FEM analysis is carried out in this section to verify the TSI by present formulation. The element type for the flange is 3 dimensional solid element, and shell element for the exhaust pipes. The total number of elements and nodes are 2234 and 2913 respectively. The displacement in y direction is fixed at the backside of the flange and those in x and z directions at point O are fixed to prevent the rigid-body motion (See Fig. 5). The temperature in the flange is 200℃ and it varies linearly along the pipes from T_A (200℃) to T_O (800℃). The commercial programs PATRAN and ABAQUS respectively are used for modeling and solving.

The maximum TSI by FEM is 7.190, which shows about 2.4% difference from the result shown in Fig. 7. The present formulation is in good agreement with the linear FEM analysis,

hence the beam approximation of the pipes neglecting the shell effect in the present analysis is

justified.

3.3 PARAMETER STUDIES IN TSI

The influences of the design parameters are examined by using the equations associated with the TSI. Fig. 8 shows how the TSI varies when the temperatue at the collecting point T_O increases with $T_A = 200^o C$ fixed. The temperature difference has a linear relationship with the TSI. The effect of the diameter of the exhaust pipe with a constant thickness and that of thickness of the exhaust pipe with a constant diameter are plotted in Fig. 9 and Fig. 10, respectively. The TSIs show approximately quadratic behavior with respect to the diameter and thickness of the pipe. As discussed in the section 3.2.2, the shell effect by comparison with present analysis and FEM for t=2.0mm is negligible, and remains so unless an extremely thin value of t is used. However we have not performed the analysis and the FEM computation for the case because it is not used in practice.
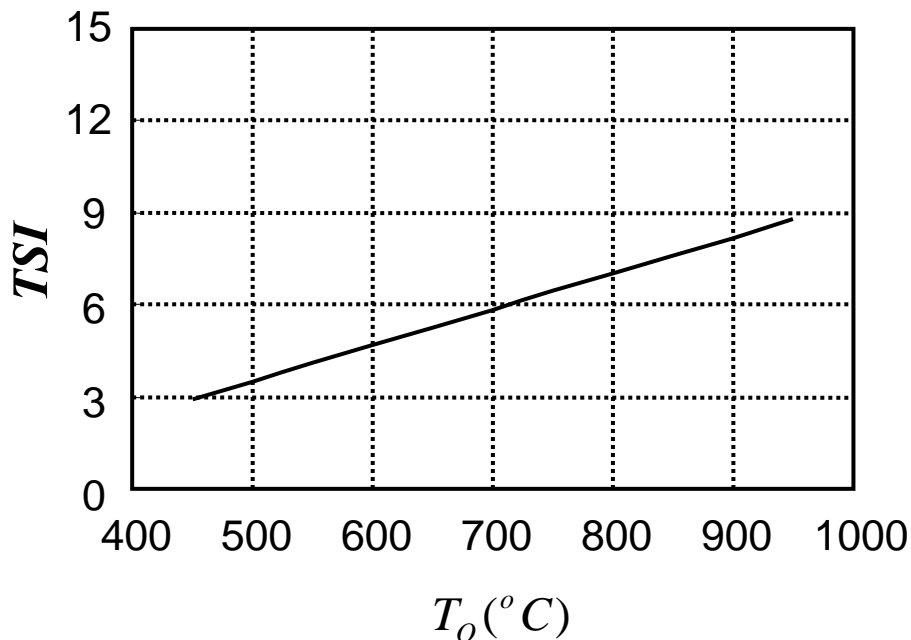
Fig. 8 *TFDI* vs. the temperature difference (with $T_A = 200^o C$)
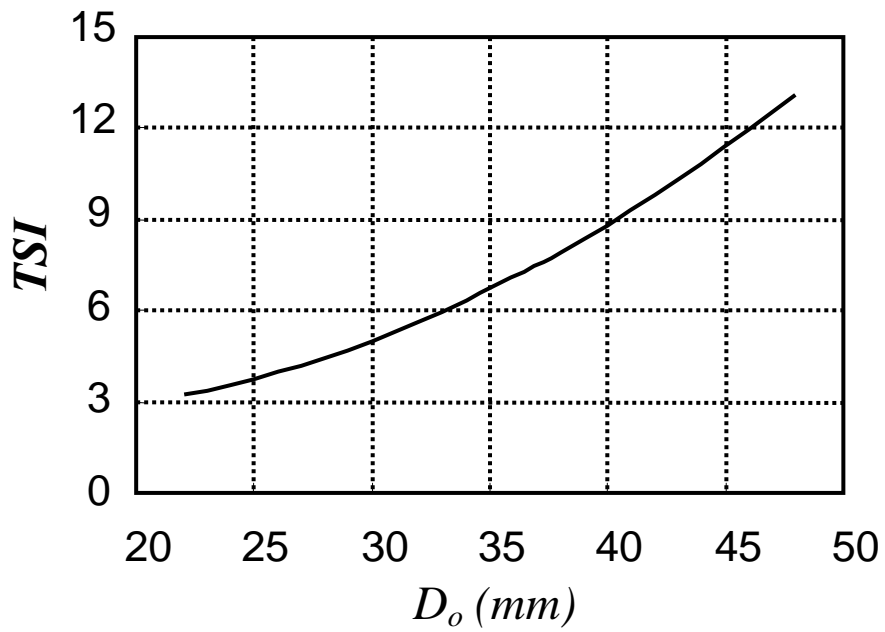
Fig. 9 *TFDI* vs. the pipe diameter (with t=2.0 mm)
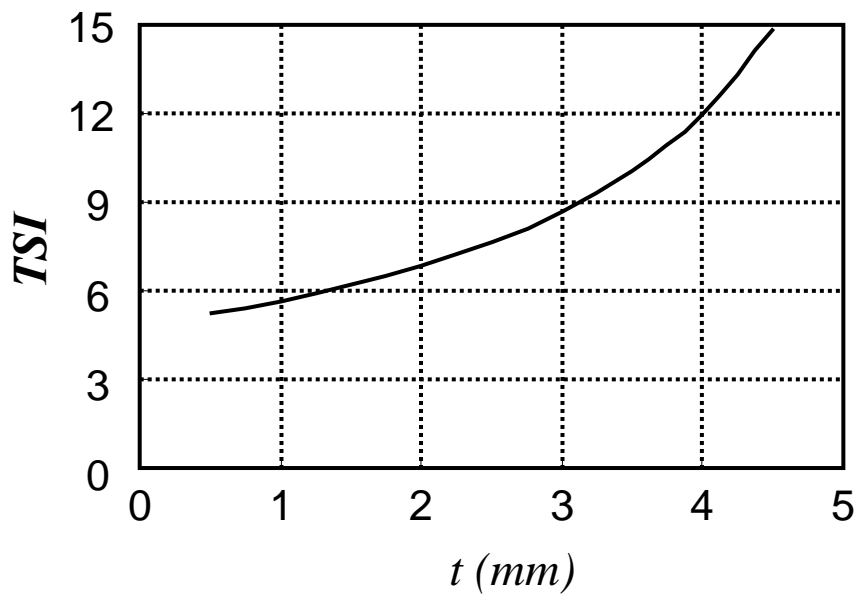
Fig. 10 *TFDI* vs. the pipe thickness (with D_o =36.5 mm)

4 DISCUSSION

It is very common in a design stage that the selection of material is restricted and the gas temperature in the exhaust manifold is limited to a certain value due to the factors affecting the performance of an engine. The useful way to increase the durability of the exhaust manifold is then a parametric study of the geometry with the given temperature and materials. F.E.M. analysis for the parametric study should include a nonlinear thermo-elastoplastic analysis in order to evaluate the fatigue life. This approach, requiring the vast amount of time in pre and post-processing, is not desirable in practice because of the lack of development time.

The calculation for the TSI requires much less time than F.E.M. analysis since the shape of the exhaust pipe $r(s)$ is only needed to evaluate the TSI. In order to get an insight into the practicality of the present analysis, we computed TSI vs. plastic strain range $\Delta\varepsilon_p$ by applying the cyclic temperature loading (i.e., from $T_O=800℃$ → $T_R=20℃$ → $T_O=800℃$ for point O, and $T_A=200℃$ → $T_R=20℃$ → $T_A=200℃$ for point A). By changing the geometrical dimensions such as D_0, and t the values TSI, and $\Delta\varepsilon_p$ so obtained are plotted in Fig.11 (we omitted the details of the numerical procedures for Fig.11). We have not computed the case of $\Delta\varepsilon_p=0$, for which D_0, and t are beyond the typical values in practical use. It is noted here that $\Delta\varepsilon_p=0$ does not imply $\varepsilon_p=0$.

It is hence concluded that the TSI suggested in this paper is helpful in predicting the durability of the exhaust manifold. An optimum shape of the exhaust manifold in an engine design also can be achieved by minimizing the TSI. It is remarked here that the TSI computed in this study is based on the linear-elasticity neglecting the cyclic nature of the material's plastic

behavior, hence, the absolute value of the TSI per se can not be used as a criterion for the rapid failure or the quantitative prediction of fatigue life. When the exhaust manifolds join together at point O as in Fig. 5, there seems to be the stress concentration. However, in practice they joint smoothly, so that we neglect the stress concentration in this study. If the nonlinear behavior related with the temperature, corrosion, oxidation and welding is additionally taken into account the result would be more accurate, which is beyond the scope of the present study. It is believed that the present study can be a guide to such models in the future.
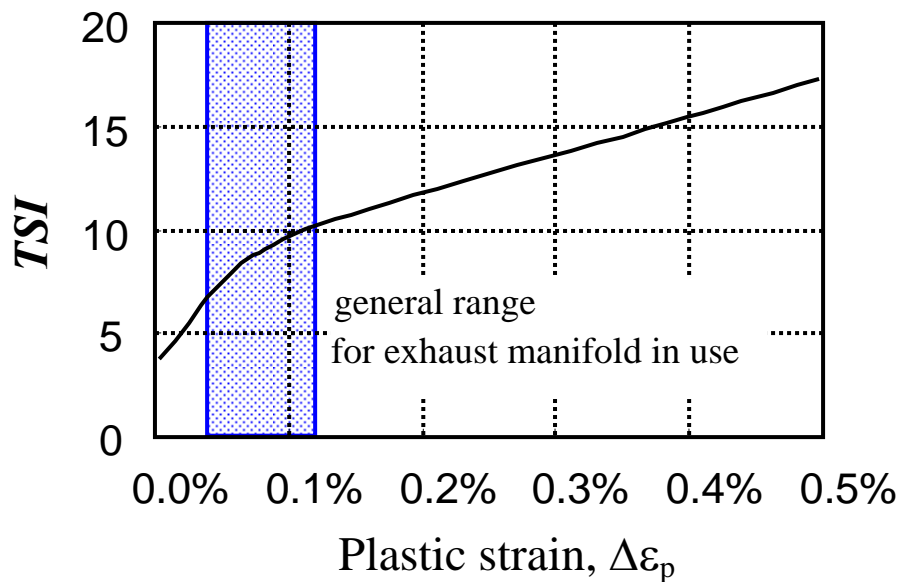
Fig. 11 TSI vs. plastic strain range, $\Delta\varepsilon_p$

5 CONCLUSIONS

(1) The thermal stress index (TSI) is developed for a general shape of the exhaust manifold to be used as a guide in selecting the manifold. The analysis is in good agreement with the FEM result.

(2) The influences of the geometric parameters, the only factors easily controlled by a designer can be evaluated within a reasonably short time in the design stage, hence, this TSI is a useful indicator for the selection of the manifold in the early stage of design. If the measured fatigue life database is used together with the TSI, this would strengthen the power of the TSI concept.

References

1 **Indig, H.** and **Williams, T.R**. Exhaust System Accelerated Durability Testing. *SAE840503*, 1984.

2 **Noguchi, T., Yasuki, T., Nakakubo T.** and **Atsumi T.** Thermal Stress and Deformation Analysis of Exhaust Manifold of Internal-Combustion Engine. *JSAE Review*, 1985, April, pp 34~39.

3 **Kawano, H., Inoue S., Iwata M., Yamaguchi, T., Yanagisawa H.** and **Fukumori E.** Improvement in the Thermal Elasto-Plastic FEM Model Applied to Exhaust Manifold. *SAE Technical Paper Series*, No. 911771, 1991.

4 **Anderson, D.H., Bisaro, D.R., Haan, D.M.** and **Olree, M.** A Thermoviscoplastic FE model for the Strain Prediction in High Temperature, Thermal Cycling Applications for Silicon Molybdenum Nodular Cast Iron. *SAE technical paper series*, No. 980697, 1998.

5 **Lederer, G., Charkaluk, E., Verger, L.** and **Constantinescu, A.** Numerical Lifetime Assessment of Engine Parts Submitted to Thermomechanical Fatigue, Application to Exhaust Manifold Design. *SAE2000-01-0789*, 2000.

6 **Shimizu, T., Takahashi, T., Ohtani, M.** and **Satake, T**. Exhaust manifold Heat Analysis. *JSAE 9531200*, 1995, pp. 181~186.

7 **Ishii, K., Nakada, M., Takahashi, S., Enomoto, M.** and **Konishi, Y.** Evaluation of Thermal Fatigue Life on the Exhaust Manifold by Analyzing Restraint Ratio. *Fista Congress*, 2000, 6.

8 **Wolff, K.** and **Huser, M**. Computer Aided Development of Exhaust System Durability. *GPC*, 1998.

9 **Japanese Industrial Standard,** JIS G 4304, Hot rolled strainless steel plate, sheets and strip (SUS429), 1999.

Appendix

Using the force and moment equilibrium, it is seen that the force f_A and the moment m_A at the end point A are related with N, V, M and T as follows:

(a) axial force (N)

$$N = E\varepsilon_N A_O = \xi \cdot f_A \tag{A1}$$

(b) lateral force (V)

$$V = \chi G \varepsilon_T = \left| f_A - (f_A \cdot \xi)\xi \right| \tag{A2}$$

(c) bending moment (M)

$$M = EI_o(\xi \times \tilde{K}) = \{\xi \cdot m_A + \xi \cdot [r_A - r(s)] \times f_A\}\xi \tag{A3}$$

(d) twisting moment (T)

$$T = GJ \frac{d\rho}{ds}\xi = m_A + [r_A - r(s)] \times f_A - \{\xi \cdot m_A + \xi \cdot [r_A - r(s)] \times f_A\}\xi \tag{A4}$$

Here, E, G, A, ρ and χ respectively are the Young's modulus, shear modulus, area of cross section, twisting angle and shear coefficient.

The total elastic energy for a curved member due to external forces is expressed as

$$\Phi = \frac{1}{2}\int_O^A \frac{N^2}{EA_o}ds + \frac{1}{2}\int_O^A \frac{V^2}{\chi GA_o}ds + \frac{1}{2}\int_O^A \frac{M^2}{EI_o}ds + \frac{1}{2}\int_O^A \frac{T^2}{GJ}ds . \tag{A5}$$

Substituting equations (A1) ~ (A4) into equation (A5) leads to

$$\Phi = \frac{1}{2}\int_O^A \frac{(\xi \cdot f_A)^2}{EA_o} ds + \frac{1}{2}\int_O^A \frac{\left| f_A \{ \underline{I} - \xi \otimes \xi \} \right|^2}{\chi GA_o} ds$$

$$+ \frac{1}{2}\int_O^A \frac{\left| m_A + [r_A - r(s)] \times f_A - \{ \xi \cdot m_A + \xi \cdot [r_A - r(s)] \times f_A \} \xi \right|^2}{EI_o} ds \qquad (A6)$$

$$+ \frac{1}{2}\int_O^A \frac{\left| \{ \xi \cdot m_A + \xi \cdot [r_A - r(s)] \times f_A \} \xi \right|^2}{GJ} ds.$$

Rewriting equation (A6) with the indicial notation,

$$\Phi = \frac{1}{2}\int_O^A \frac{(\xi_i f_i)(\xi_j f_j)}{EA_o} ds$$

$$+ \frac{1}{2}\int_O^A \frac{f_i f_i - \xi_i \xi_j f_i f_j}{\chi GA_o} ds$$

$$+ \frac{1}{2}\int_O^A \frac{m_i m_i + 2m_i \varepsilon_{ijk}(R_A)_j f_k + (R_A)_i (R_A)_i f_j f_j - (R_A)_i (R_A)_j f_i f_j}{EI_o} ds \qquad (A7)$$

$$+ \frac{1}{2}\int_O^A (\frac{1}{GJ} - \frac{1}{EI_o})\left[\xi_i m_i + \xi_i \varepsilon_{ijk}(R_A)_j f_k \right]^2 ds$$

where $(R_A)_i$ $(i = 1,2,3)$, f_i $(i = 1,2,3)$ and m_i $(i = 1,2,3)$ respectively are the ith component

of $R_A = r_A - r(s)$, f_A and m_A.

Table caption

Table 1   Data of the exhaust manifold used in verification program

Figure caption

Fig. 1   Schematic configuration of the simplified exhaust manifold

Fig. 2   A curved member in a space

Fig. 3   Schematic diagram of the cylinder head

Fig. 4   Definition of the coordinate axis

Fig. 5   Geometry of exhaust manifold for analysis

Fig. 6   The geometry of the exhaust pipe for the calculation of TSI

Fig. 7   Thermal fatigue damage index number

Fig. 8   TSI vs. the temperature difference (with $T_A = 200^o C$)

Fig. 9   TSI vs. the pipe diameter (with t=2.0 mm)

Fig. 10 TSI vs. the pipe thickness (with D_o =36.5 mm)

Fig. 11 TSI vs. plastic strain range, $\Delta \varepsilon_p$

Table 1. Data of the exhaust manifold used in verification program

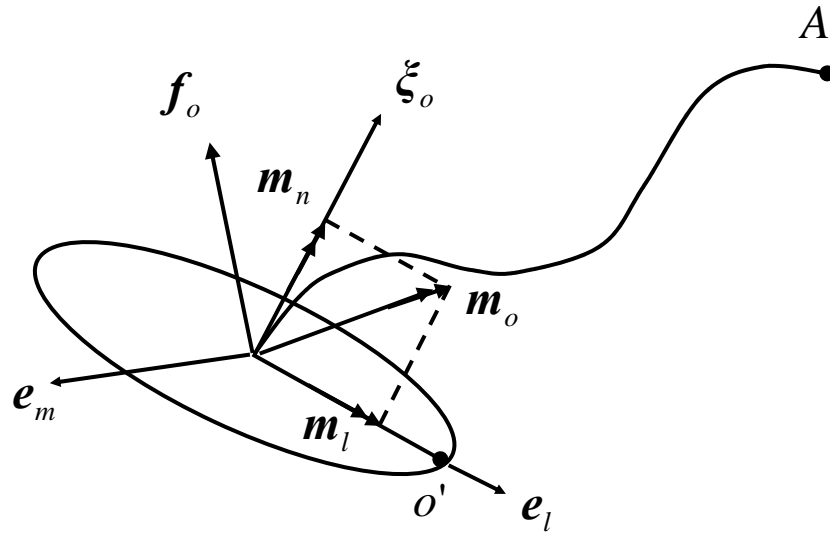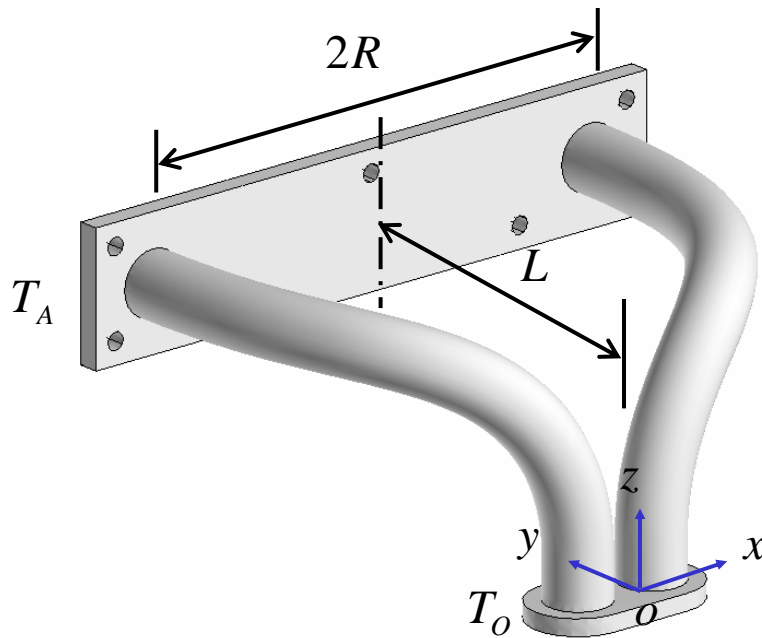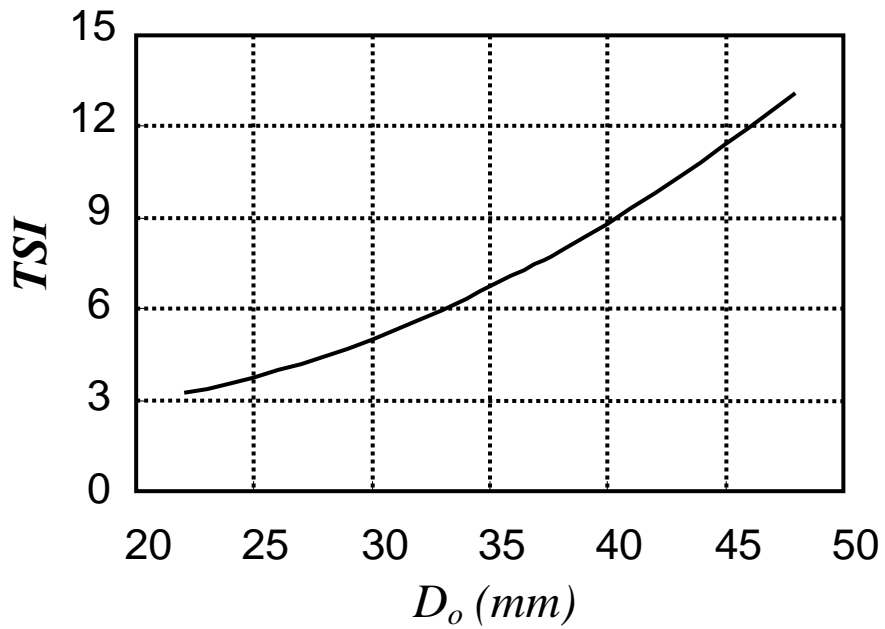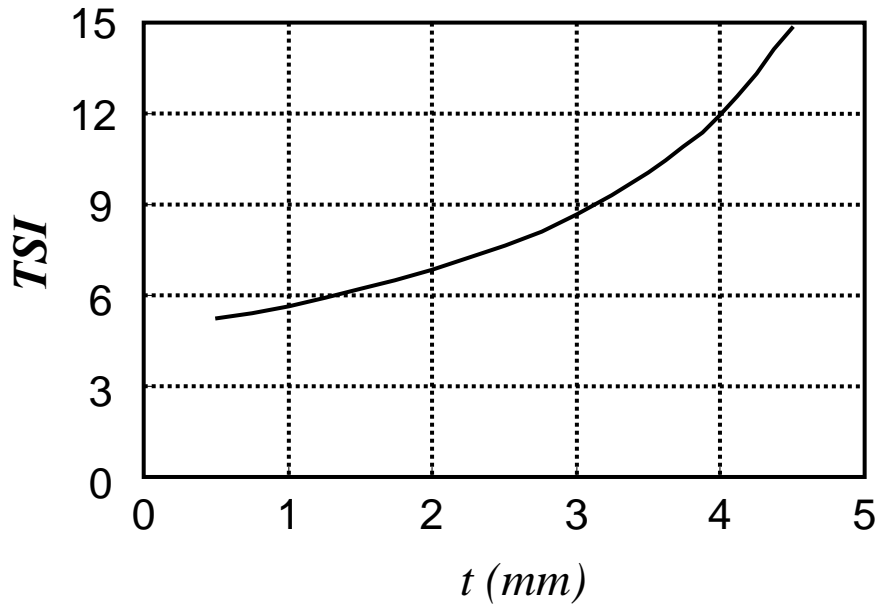| Geometry		Temperature		Material Property (SUS429EM [9])	
R	144mm	T_A	200℃	E	193 (GPa)
L	200mm	T_O	800℃	σ_y (800℃)	23 (MPa)
t	2.0mm	T_R	20℃	σ_y (20℃)	336 (MPa)
D_o	36.5mm			$\hat{\alpha} = \alpha$	10.4×10^{-6} (1/K)

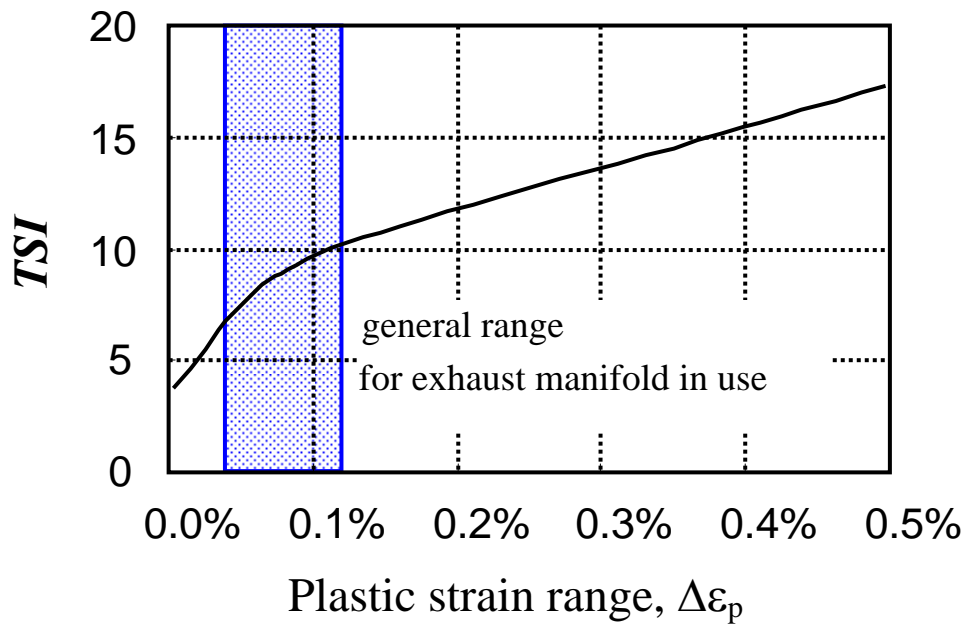K.H. Park *et al.*
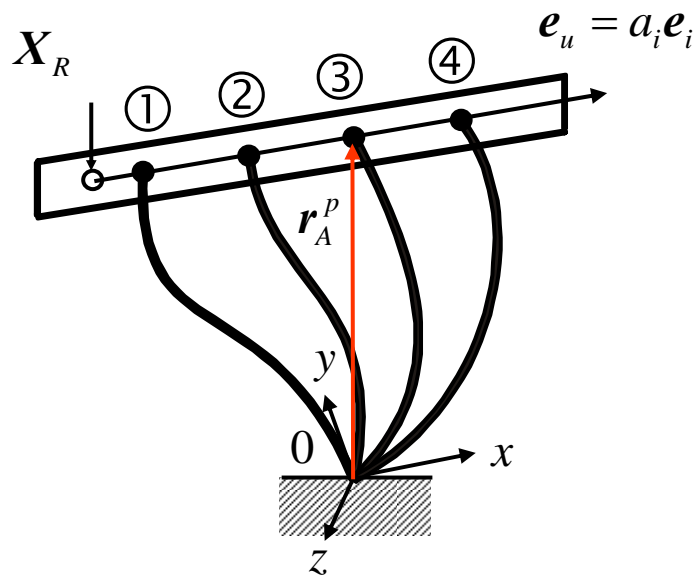
Fig. 1
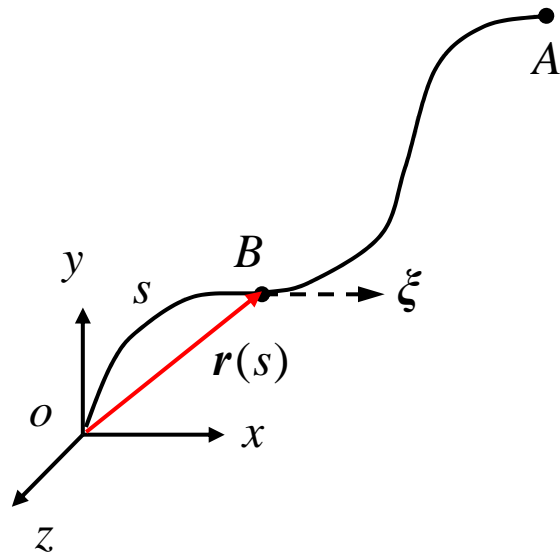
Fig. 2
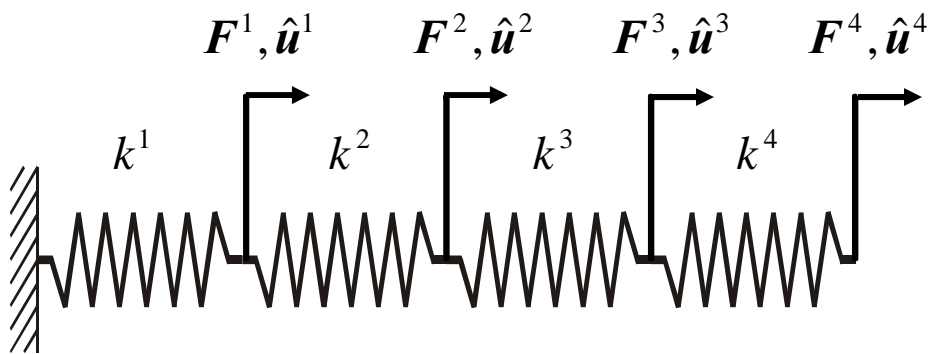
Fig. 3

Fig. 4

Fig. 5
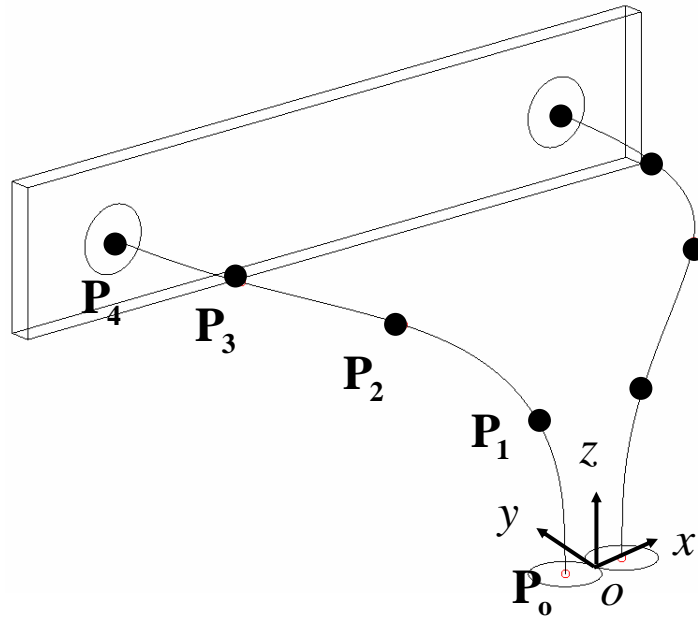
Fig. 6

Fig. 7

Fig. 8

Fig. 9

Fig. 10

general range
for exhaust manifold in use

Plastic strain range, $\Delta\varepsilon_p$

Fig. 11